OFDM-based Synchronous PNC Communications Using Higher Order QAM Modulations*

Ehsan Atefat Doost, Firooz B. Saghezchi, Shahid Mumtaz, Jonathan Rodriguez
Instituto de Telecomunicações, Universidade de Aveiro
3810-193 Aveiro, Portugal
{e.atefatdoost, firooz, smumtaz, jonathan}@av.it.pt

Leila Musavian
School of Computer Science and Electronic Engineering, University of Essex
Colchester CO4 3SQ, U.K.
leila.musavian@essex.ac.uk

***Abstract*—Physical-layer Network Coding (PNC) has great potential to improve the throughput and latency in wireless networks. However, there are two main challenges in PNC systems that do not exist in the conventional Point-to-Point (P2P) communication systems: 1) time and frequency asynchrony of the paired PNC users; and 2) ambiguity of the PNC mapping at the relay node. To address these challenges and aiming at further improvement of the spectral efficiency of the PNC-enabled wireless networks using higher-order modulations, in this paper, we apply precoding for power control and phase synchronization of the paired PNC users. Furthermore, we employ modulo-$\sqrt{M}$ addition for the PNC mapping ambiguity removal in M-QAM (Quadrature Amplitude Modulation) constellations. We evaluate the performance of the system in the framework of the Orthogonal Frequency Division Multiplexing (OFDM)-PNC systems with cyclic prefix extension under both Additive White Gaussian Noise (AWGN) channel and Rayleigh faded TDL-C and TDL-D (Tapped Delay Line) channel models proposed by the Third Generation Partnership Project (3GPP). The results reveal that for the case of Binary Phase Shift Modulation (BPSK), our proposed technique can achieve a significant Signal-to-Noise Ratio (SNR) improvement of 12 dB over its asynchronous OFDM-PNC counterpart (without precoding) under a TDL-C faded channel. Moreover, the proposed solution attains a Bit Error Rate of 10^{-3} for 16-QAM at the SNR of around 13dB.**

Keywords—Physical-layer Network Coding, PNC Mapping, Ambiguity Removal, Synchronous PNC, Precoding, QAM.

I. INTRODUCTION

Physical layer Network Coding (PNC) was first proposed by Zhang et. al., [1] and Popovski et. al. [2], independently in 2006, to efficiently exchange data between two paired users over a two-way relay channel. The users transmit their data simultaneously and the relay decodes and forwards the received signal, which is the superposition of the transmitted signals by the two paired users. However, in PNC systems, the relay needs to identify the exact starting samples of the packets of the two end nodes for the decoding purpose [3]. Moreover, the users need to unambiguously recover the data of their paired partner based on the coded data that they receive from the relay. This requires to accurately estimate and compensate for the two channel responses from the paired users to the relay. Thus, two major challenges emerge in PNC systems that do not exist in conventional point-to-point (P2P) communication systems [3], [4]: 1) time and frequency synchronisation of the paired users; and 2) ambiguity removal resulted from the PNC mapping and/or the channel fading.

Essentially, there are two types of asynchronies in PNC systems: 1) time asynchrony: for which packets are sent simultaneously by the two paired users (UE_1 and UE_2), but they do not necessarily arrive at the relay at the same time; and 2) frequency asynchrony: where there is a relative phase and frequency offset between the local oscillators of UE_1 and UE_2 [4], [5]. To deal with these asynchronies, two main types of PNC frameworks exist in the literature [4], [5]: 1) synchronous PNC; and 2) asynchronous PNC. Synchronous PNC employs pre-processing mechanisms such as time advance transmission so as the symbols arrive at the relay with symbol and phase alignment. In contrast, asynchronous PNC does not perform any pre-processing, rather it employs receiver-side postprocessing such as Belief Propagation (BP) algorithm [6] or modifies the frame's preamble in Orthogonal Frequency Division Modulation (OFDM) systems to relax the tight synchronization, allowing symbol misalignment within Cyclic Prefix (CP) length [4], [7].

In the PNC mapping operation, ambiguity arises from two main factors 1) mapping algorithm ambiguity, especially for higher-order modulations (e.g, bitwise exclusive-or (XOR) in 16-QAM [8]); and 2) channel fading effects which cause relative phase rotation of the two transmitted symbols at each subcarrier, especially, in frequency selective channels, the so-called *singular fade state* (SFS) causes distance shortening problem in the signal constellation received at the relay [9].

This paper addressed the synchronization and ambiguity removal challenge in PNC systems using higher-order QAM modulations. In particular, the main contributions of this paper can be summarized as follows:

- Most of the existing studies on the OFDM-PNC adopt an Additive White Gaussian Noise (AWGN) channel or a simple two- or three-path Rayleigh fading channel to keep the problem analytically tractable. However, in this paper, we implement OFDM-PNC in the presence of more realistic 5G channel models proposed by 3GPP [10]. In particular, we study UMi (Urban Micro-cell) TDL-C (Rayleigh faded) and TDL-D (Rician faded) channels and evaluate the performance of the OFDM-PNC to characterize its attainable performance limit under practical channel constraints.
- To improve the spectral efficiency of the OFDM-PNC systems, we implement a generalizable PNC mapping that is applicable not only to BPSK but also to higher-order QAM modulations (16-QAM, 64-QAM, etc.) and apply precoding for synchronization and channel ambiguity removal. We assess the performance of the system for BPSK, 4-QAM, and 16-QAM and compare the results with a benchmark OFDM-PNC system without using precoding. Since conventional XOR

*This work has been funded partly by the European Union Horizon 2020, RISE 2018 scheme (H2020- MSCA-RISE-2018) under the Marie Skłodowska-Curie grant agreement No. 823903 (RECENT) and partly by the Fundação para a Ciência e a Tecnologia (FCT-Portugal) with reference No. 2021.08263.BD.

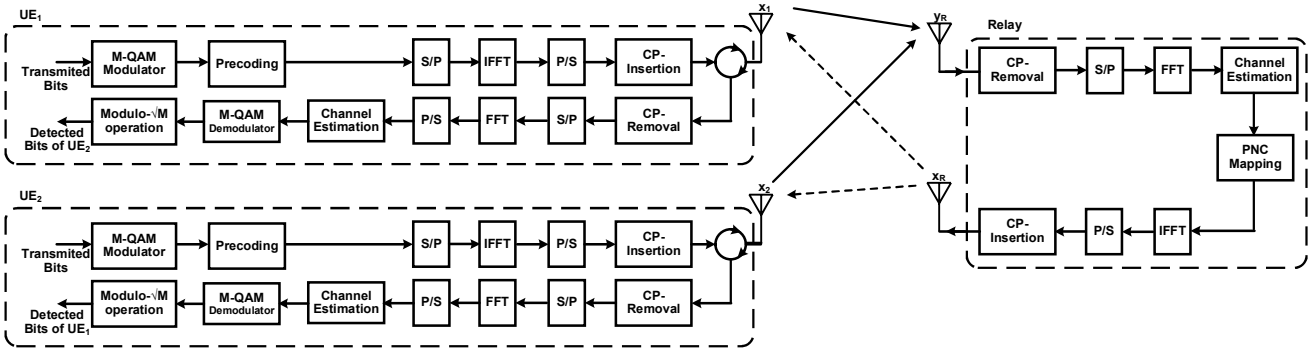

Fig. 1. Baseband block diagram of the considered OFDM-based PNC communication system with two UEs (UE_1 and UE_2) and one relay, including the tranmitting and receiving signal processing chains. S/P and P/S stands for serial to parallel and prallel to serial conversion operations, respectively.

operation for PNC mapping results in ambiguity for M-QAM modulation with $M \geq 4$ [8], we adopt the constellation-based mapping technique proposed in [11] for higher-order QAM modulations, which reduces to simple XOR mapping in the case of BPSK.

The rest of this paper is organized as follows. Section II reviews the state-of-the-art. Section III presents the system model, while the simulation setup and the evaluation results are presented in section IV. Finally, Section V concludes this paper and draws guidelines for the future work.

II. Related Work

To overcome the ambiguity originated from the mapping algorithm, [8] and [11] proposed a PNC mapping algorithm for higher-order QAM modulations. However, their method suited only for synchronous PNC systems where the channels of the paired UEs are symmetric and have no relative phase offsets, such as the case in AWGN channels. However, for multipath fading channels, some preprocessing is required at the paired UEs to synchronize and compensate for the channel phase distortion effect. This is further elaborated and implemented later on in our system model.

For the purpose of explanation, suppose that H_1 (H_2) is the frequency response of the channels between UE_1 (UE_2) and the relay. The ratio $z=\frac{H_2}{H_1}=\gamma.e^{j\theta}$ is called *channel fade state*, which is usually used to characterize the channel-induced ambiguity, resulting from its Singular Fade States (SFSs) [9]. To resolve the channel-induced ambiguity, two main mechanisms have been proposed in the literature: 1) transmitter-side policies, which includes space-time coding [12], [13], precoding [14], [15], [16] and multiple antenna techniques [9]; and ii) receiver-side policies, which includes the Closest-Neighbor Clustering (CNC), the Nearest-Neighbor Clustering (NNC) [17] and the Latin Square technique [18]. Among these SFS removal techniques, precoding is easy to implement and achieves higher spectral efficiency for a given transmit power [13]. It also requires less computational cost for the relay and ensures power control at the paired PNC users, which is essential for the operation of the PNC systems.

Two precoding schemes namely channel inversion and blind subcarrier suppression (BSS) was proposed in [14] for OFDM-PNC. In [12], the authors proposed a scheme called Distributed Space-Time Coding (DSTC), which uses constant precoding matrices, hence it does not need any channel state information (CSI) knowledge at the transmitting nodes (CSIT). Their proposed scheme attains a good performance in higher SNRs. The drawback of the DSTC scheme is that it is designed to handle multiple-access interference only, and it does not work well when one or more channels from the terminal nodes to the relay are in deep fade [13]. To overcome this shortcoming, the authors of [13] proposed a general form of DSTC algorithm called distributed linear constellation precoding (DLCP), which uses OFDM signaling to achieve multipath diversity while handling multiple access interference. The work in [15] implemented a precoding-assisted PNC scheme using lattice network coding on software-defined radios (SDR). It uses low-density lattice codes decoder to deal with the channel misalignment and supports higher-order modulations in static or low mobility scenarios. However, its implementation requires high dimensional lattice codes whose dimension increases exponentially with the modulation order and it is highly complex for resource constraint UEs. Denho et al. [16], proposed a spatial precoding-based PNC with higher order M-QAM in MIMO OFDM communications. However, their proposed technique requires $N_R \geq 2$ relay nodes in each PNC transmission [16].

Different from aforementioned schemes, in this paper, we combine both channel SFS removal and PNC ambiguity resolving schemes to come up with a more robust solution for multipath fading scenarios. The use of M-QAM modulation is indispensable in wireless PNC to further improve the SE. For removing channel-induced SFS effects, we use a precoding mechanism that essentially transforms a multipath fading channel to an effective AWGN channel (perceived by the relay) to accommodate higher order M-QAM modulations. In addition, to remove the PNC mapping ambiguity, we use the constellation-based mapping technique proposed in [11] for higher-order QAM modulations.

III. System Model

A. PNC Signaling

Fig. 1 depicts the overview of our system model. For the PNC signaling, we adopt the method proposed in [1], where the two-way packet exchange is executed in two phases: 1) multiple access (MA) phase; and 2) broadcast (BC) phase. The process flow of these two phases is as follows.

Phase 1: Multiple Access Phase

At the beginning of phase 1, the relay node begins with time synchronization of the two paired UEs to ensure synchronous arrival of their signals at the relay. We use the

signaling proposed in [4], which allows the two signals to be slightly misaligned (within CP duration). As shown in Fig. 1, the baseband signal processing is as follow. Both the paired UEs (UE_1 and UE_2) use the same M-ary QAM modulation to modulate their binary data drawn from two independent and identically distributed Gaussian codebooks, i.e.

$$X_j=\text{Modulate}\,(b_j),\ j\in\{1,2\}, \qquad (1)$$

where b_j is the binary data message of the j-th user, $j\in\{1,2\}$. To compensate for the channel time offset, which results in phase rotation of the two transmitted constellations of UE1 and UE2, precoding mechanism that is presented in subsection III.A is performed in this stage. We use IEEE 802.11 frame format, with 64 subcarriers, including 48 data subcarriers along with four BPSK pilot signals inserted into subcarriers 1, 16, 31 and 46 of each frame to track the channels between the two UEs and the relay [4].

Performing precoding, the two paired UEs send their (time-domain) signals x_j (j=1,2) with a certain time advance such that they can arrive at the relay aligned within the CP duration time. That is, their misalignment is not larger than the CP duration. Assuming frequency flat fading channels and single antenna transceivers for the UEs and relay, the received signal at the relay is the superposition of the Electromagnetic (EM) signals emitted by the J=2 active UEs, i.e.:

$$y_R[n]=\sum_{j=1}^{J=2} h_j * x_j + n_r. \qquad (2)$$

where n_r is the AWGN with mean zero and variance σ^2, and h_j, j=1,2 is the channel impulse response between UE_j and the relay, modelled as a Time Delay Line (TDL) [4]:

$$h_j[n]=\sum_{l=1}^{L} h_j^l.\delta[n-\tau_j^l]. \qquad (3)$$

where $h_j=\left[h_j^0, h_j^1, \ldots, h_j^{L_j-1}\right]$ represent the fading coefficients of the channel with L_j taps, $\sum_{l=1}^{L}\left|h_j^l\right|^2=1$, and τ_j^l (l=0, 1, …L_j; $\tau_j^l-\tau_j^0=\tau_l$) is the normalized path delay.

The channel gains h_j^l can be expressed as follows [19].

$$h_j^l=g_j.\sqrt{\beta_j} \qquad (4)$$

We assume that the channels are reciprocal (i.e., h_j uplink$=h_j$ downlink), with mean square fade coefficient $\overline{\left|h_j\right|^2}=1$ (j=1,2) that is assumed to be slow and flat fading. In other words, the transmission time (two slots/frames) is limited within the channel coherence time. Furthermore, for the j^{th} user, g_j represents a small-scale fading model, which is drawn from a Rayleigh/Rician distribution. The parameter β_j depicts the large-scale fading coefficients that represents both path loss (PL_j) and shadowing effects (χ_j).

At the relay, as shown in Fig. 1, the receiver first performs the serial to parallel conversion and then takes an N-point FFT. As proved in [4], in OFDM-PNC, if the length of the CP is larger than the maximum channel delay spread of the two paired UEs denoted as $L=\max\{L_1, L_2\}$ (i.e., if CP> L), the symbols are still aligned in the frequency domain (i.e., the symbol misalignment in the time domain is translated to phase offset in the frequency domain that can be compensated by the precoder). Hence, after removing CP and performing the N-point FFT, the received signal at the relay in the frequency domain becomes [4]:

$$Y_R[k]=\sum_{j=1}^{J} H_j[k].X_j[k]=H_1[k].X_1[k]+H_2[k].X_2[k]+N_R[k],$$

$$k=0,1,\ldots,N-1. \qquad (5)$$

Phase 2: Broadcast Phase

As can be seen from Fig 1, phase 2 starts by channel estimation process using block-type and comb-type pilots inserted into the preamble and data parts of the frame, respectively [4], which is followed by joint channel decoding and PNC mapping as described below in Subsection III.B. After these operations, a symbol-wise modulo-M′ addition (where, $M'=\sqrt{M}$) of the paired users' data frames is performed, as the PNC mapping operation, which is generally denoted as $Z=f(x_1, x_2)$. The outcome is then modulated at the relay on the OFDM waveform, and the modulated signal (X_R) is broadcast toward the paired UEs. At the UEs, as shown in Fig. 1, each UE detects $\widehat{Z}=\hat{f}(x_1, x_2)=\widehat{x_1 \oplus x_2}$ using channel estimation and equalization as explained in [4]. Then, with the knowledge of its own transmit symbol x_1 (x_2), and by performing the XOR operation of $\widehat{x_1 \oplus x_2}$ and x_1 (x_2), UE_1 (UE_2) obtains the symbol transmitted by its peer. It should be noted that for higher order modulations, instead of XOR operation, modulo- $M'=\sqrt{M}$ operation is performed, as elaborated in the following in Subsection III.B.

A. Precoding

Precoding mechanism is based on channel inversion [14] and has the following stages.

1. Both paired UEs (UE_1 and UE_2) send their packets which include time orthogonal pilot sequence (Xp(k), k=1,…,64) to the relay.
2. Relay performs channel estimation for each of the UEs and feed backs the separated channel estimates of H_1 and H_2 to the transmitting UEs. Assuming that the channel is reciprocal, which is typically the case for the systems operating in the time-division duplex (TDD) mode (which is the case for our PNC system), the estimated channel can be used for both MA and BC communications in our PNC system.
3. Each of the paired UEs performs channel inversion-based precoding, i.e., UE_1 (UE_2) sends $X_1[k].\frac{1}{H_1[k]}$ ($X_2[k].\frac{1}{H_2[k]}$) to the relay. Through this precoding, the equation (5) is simplified as:

$$Y_R[k]=X_1[k]+X_2[k]+N_R[k]. \qquad (6)$$

Hence, employing precoding, the received signal at the relay becomes simply the sum of the two transmitted signals (in the frequency domain) impaired by an AWGN channel, thus neutralising the channel fading artefacts. As such, the same detector used in an AWGN channel can be used for detecting the signal affected by a fading channel. We discuss this further in the following subsection.

B. PNC Mapping

For BPSK modulation, we use PNC mapping operation presented in [4], while there is no precoding operation. For M-QAM modulations, the precoding mechanism is employed such that the PNC mapping presented in [11] can be used, and since the in-phase and quadrature components of the (square-shaped) M-QAM signal is a $\sqrt{M}$–ary PAM signal, we perform the PNC mapping operation on each of these $\sqrt{M}$–ary PAM signals.

1) PNC Mapping for 4-QAM modulation

4-QAM signal is essentially composed of two $M'=\sqrt{M}=2$-ary PAM signals; therefore, we first derive the In-Phases (I) and Quadrature (Q) components of the received signal at the relay and then perform the detection and PNC mapping operations on each of these components separately.

Using the precoding mechanism explained above in subsection III.A, an effective AWGN channel is established for fading channels, and hence the real part of the composite received signal at the relay becomes:

$$Y_{R,I}[k]=X_{1,I}[k]+X_{2,I}[k]. \qquad (7)$$

To focus on the PNC mapping operations, we ignore the noise contribution temporarily, later we will add its effects to our calculations. In the case of $M'=\sqrt{M}=2$ (2-PAM modulated data), as shown in Fig. 2a, the Euclidian distance between neighboring constellations is $d=\sqrt{E_b}$ [20], where d is voltage level assigned to each level of PAM pulses, and E_b represents the energy of each bit level. In Fig. 2a, $C_j \in \{0,1,\ldots,\sqrt{M}-1\}$ represents the constellation point indices for the transmitted symbols of UE_j , $j\in\{1,2\}$, which create the superposed signal $Y_{R,I}$ and similarly, $Y_{R,Q}$ Furthermore, d_{C_1} denotes the corresponding symbols in the constellation. As shown in Fig. 2b, the constellation of the I and Q components of the superposed received signal at the relay becomes a 3-PAM constellation (-2d, 0, 2d). Finally, Fig. 2b also shows the decision boundaries γ_1 and γ_2 for signal detection at relay.

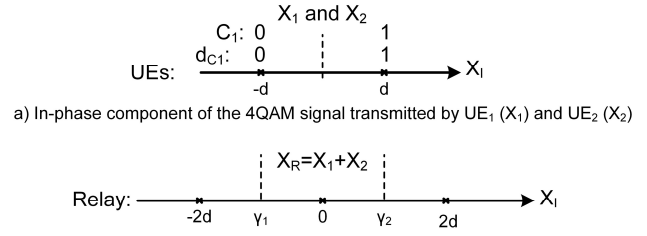

Fig. 2. Constellation and decision boundaries for PNC mapping using 4-QAM modulation at both paired UEs ($d=\sqrt{E_b}$)

As discussed in [11], the PNC mapping for the I component can be summarized as shown in Table I, where the resulted mapped data is $X_{r,I}$. Likewise, the PNC mapping for the Q component is summarized in Table II.

Combining I and Q components, the PNC mapped data corresponding to the original 4-QAM symbols can be obtained as follows.

$$X_r=X_{r,I}+jX_{r,Q} \qquad (8)$$

TABLE I. DECISION AND MAPPING RULES FOR IN-PHASE COMPONENT OF 4-QAM SUPERPOSED SIGNALS AT THE RELAY

$X_{1,I}[k]+X_{2,I}[k]$	-2d	0	2d
(C_1, C_2)	(0,0)	(0,1) (1,0)	(1,1)
$S_{r,I}=(C_1+C_2) mod\ M'$	0	1	0
$X_{r,I}$	-d	d	-d

TABLE II. DECISION AND MAPPING RULE FOR QUADRATURE COMPONENT OF QAM SUPERPOSED SIGNALS AT THE RELAY

$X_{1,Q}[k]+X_{2,Q}[k]$	2d	0	-2d
(C'_1, C'_2)	(0,0)	(0,1) (1,0)	(1,1)
$S_{r,I}=(C'_1+C'_2) mod\ M'$	0	1	0
$X_{r,Q}$	d	-d	d

Now, the transmitted signal by the relay, X_r is broadcast toward the receiving end nodes (UE_1 and UE_2). Next, as shown in Table III and in Fig. 1, each UE detects its peer's data. For instance, if UE_2 wants to detect UE_1's data, using its own transmit symbol constellation indices (i.e., C'_2), and by performing $(\hat{S}_{r,Q}-C'_2) \bmod M'$ operation, as summarized in Table III, the indices of the received symbol constellation $\hat{C}'_1$ is estimated, and UE_1's data symbols are obtained at UE_2.

TABLE III. DECISION AND MAPPING RULE FOR IN-PHASE COMPONENT OF QAM SIGNALS AT THE RECEIVING NODES

$\hat{Y}_{2,I}[k]=\hat{X}_{r,I}$	-d	d	-d
$\hat{S}_{r,I}$	0	1	0
$\hat{C}'_1=(\hat{S}_{r,I}-C_2) mod\ M'$	?	?	?

TABLE IV. DECISION AND MAPPING RULE FOR QUADRATURE COMPONENT OF QAM SIGNALS AT THE RECEIVING NODES

$\hat{Y}_{2,Q}[k]=\hat{X}_{r,Q}$	d	-d	d
$\hat{S}_{r,Q}$	0	1	0
$\hat{C}'_1=(\hat{S}_{r,Q}-C'_2) mod\ M'$	?	?	?

For PNC mapping in BPSK (2-PAM) modulation, only the I-component of the abovementioned algorithm is applied.

2) PNC Mapping for 16-QAM modulations

16-QAM signal constellation is composed of two $M'=\sqrt{M}=$ 4-PAM signals, therefore through procedures similar to the 4-QAM modulation, the superposed I and Q components are calculated, and the corresponding PNC-mapping operation is performed on each component. In the case of M=4 (4-PAM modulated data), the Euclidian distance between neighboring constellations is $d=\sqrt{2E_b/5}$ [20]; furthermore, assuming d=1, the $E_b=\sqrt{5/2}$.

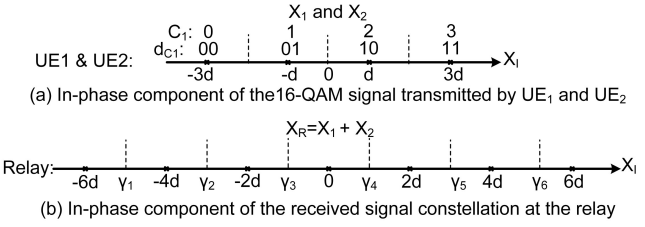

Fig. 3. Constellation and decision boundaries for PNC mapping using 16-QAM modulation at both paired UEs ($d=\sqrt{2E_b/5}$)

The PNC mapping calculations for 4-QAM modulation explained above is generalizable by the same logic to any higher order M-QAM modulation (e.g., 16-QAM, 64-QAM). For brevity, we excluded the mapping tables for 16-QAM.

IV. Performance Evaluation Results

Since the BER of PNC systems is dominated by the uplink phase, due to synchronization and PNC mapping errors, we study only the BER contribution of the uplink phase in our simulations. For example, assuming UE_2 wants to detect UE_1's data, the overall system performance is evaluated using PNC mapping output at the relay and performing modulo-M′ addition of this output symbols with UE_2's own transmit symbol constellation indices (i.e., C'_2). As shown in Table III, the indices of the received symbol constellation $\widehat{C}'_1$ are estimated and UE_1′s data symbols are obtained at UE_2.

We consider design parameters according to IEEE802.11p standard [20] as summarized in Table V. To have a symmetrical channel between UE_1-Relay and UE_2-Relay in terms of pathloss, for the case of without precoding scenario, channel pathloss inversion-based power control is performed (i.e., for the k-th subcarrier $p_k = 1/PL_j$ for j=1,2).

For channel model, we consider a realistic 5G channel model in Urban Micro (UMi) Street-canyon scenario. Specifically, we use the TDL-C and TDL-D models presented in [10], which represent Rayleigh and Rician fading channels, respectively. To add pathloss effects, in the UMi scenario [10], the following parameters are used in our simulations. The antenna height of the relay and UEs are $h_R = 10\,m$, $h_{UT} = 1.5\,m$, respectively. The street width is W = 100 m, the building height is h = 5 m, and the carrier frequency is fc=4 GHz. We also benchmark the results for our considered TDL-C and TDL-D channels against an AWGN channel.

TABLE V. Simulation Parameters

Parameters	Value	
Bandwidth	10 MHz for OFDM	
No of antennas	At relay	1
	Per UE	1
No of UEs (J)	2	
Channel model, h_j	TDL-C (Max Delay spread Dmax=1.58 µs(<CP))	
	TDL-D (Max Delay spread Dmax=1.56 µs(<CP)). The first tap follows the Rician distribution with K-factor of 13.3 dB and a mean power of 0 dB.	
	AWGN	
Distance (space) between subcarriers (Δf=B/Nfft)	156.25 KHz	
$T_{fft}=4*T_{CP}=T_{symbol}-T_{CP}$	64	6.4 µs
Cyclic prefix ($T_{CP}=1/(4*\Delta f)$)	16	1.6 µs
Symbol length ($T_{symbol}=T_{fft}+T_{CP}=5*T_{CP}$)	80	8 µs
Number of data Subcarriers	48	
Number of pilot subcarriers	4	
Total Number of subcarriers	64	
Modulation	BPSK, 4-QAM, 16-QAM	
OFDM symbols per super-frame	4	
Baseband (FFT) sampling rate (which is equal to channel sample rate)	10M samples/s (10 MHz)	
Up-sampling factor (USF)	10	
Data Rate	6 Mbps (BPSK), 12 Mbps (4-QAM), 24 Mbps (16-QAM)	

Fig. 4 illustrates the BER performance of BPSK modulation under TDL-C, TDL-D and AWGN channels. As can be seen from the figure, the BER performance of a precoding-based system in a TDL-C or TDL-D channel is similar to the performance of the system without precoding under an AWGN channel. Indeed, the precoding mechanism resolves the multipath fading channels effects regardless of the multipath fading scenario (TDL-C or TDL-D), and the same BER performances are achieved through using precoding mechanism in both symmetric and asymmetric multipath fading channels.

In addition, as can be seen from Fig. 4, for the system without precoding, the BER is very sensitive to the noise level. In particular, to achieve a BER of 10^{-3} under a TDL-C channel, the system without precoding requires around 22 dB SNR, while a precoding-based system requires only 10 dB (i.e. precoding can improve the SNR by 12 dB at the relay). However, the situation is different in a TDL-D scenario, the penalty is only around 1dB. The reason for higher performance in TDL-D scenario, in comparison to TDL-C scenario is that the TDL-D channel is dominated by the line of sight (LoS) path and has fewer multipath components leading to the SFSs of the channel.

Fig. 5 depicts the BER performance of our proposed synchronous PNC system for 4-QAM and 16-QAM modulations in the presence of TDL-C (Rayleigh) channel. For 16-QAM modulation, the higher spectral efficiency comes at the cost of slightly more required SNR. In particular, for a BER of 10^{-3}, there is a 3 dB penalty, in comparison to the 4-QAM-based PNC.

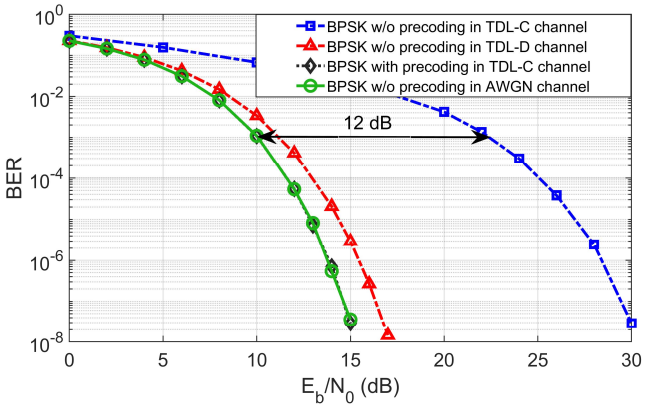

Fig. 4. BER comparison of BPSK modulation with and without precoding in TDL-C and AWGN channels

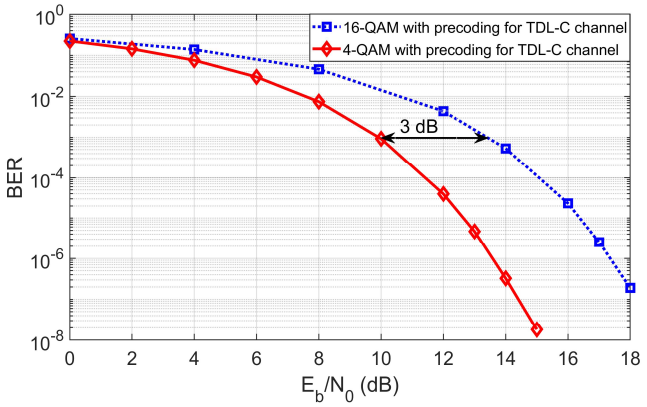

Fig. 5. BER comparison of 4-QAM and 16-QAM modulations with and without precoding in TDL-C and AWGN channels

V. Conclusion and Future Work

In this paper, we addressed the phase offset compensation in OFDM-PNC systems by employing precoding for higher order QAM modulations. The results suggest that for higher-order M-QAM modulations (M>=4), apart from using proper CP length (CP>=L), transmitter-side precoding and power control are also crucial to avoid the ambiguities stemming from the phase distortions of the MA channels and enable the relay to detect higher-order M-QAM signals with a low BER.

Exploiting our proposed precoding mechanism, the system attains the same BER performance for both multipath fading and AWGN channels. This is due to the fact that using precoding operation, the channels' phase offset, attenuation, and pathloss effects are fully compensated, hence the mutual interference of the paired transmitted signals (X_1 and X_2) in the composite signal at the relay becomes constructive. In particular, using 16-QAM modulation, the precoding assisted OFDM-PNC system attains a BER performance of 10^{-3} at an SNR of around 13 dB. Furthermore, for a BPSK modulation, the precoding-based OFDM-PNC system shows an SNR improvement of 12 dB at the BER level of 10^{-3} in comparison to its asynchronous counterpart. However, this performance comes at the cost of the availability of perfect CSI knowledge and the precoding operation at the transmitters.

For future work, this work can be extended to MIMO-PNC and mobile scenarios for vehicular communications.

References

[1] S. Zhang, S. C. Liew, and P. P. Lam. "Hot Topic: Physical Layer Network Coding," ACM MobiCom '06, pp. 358-365, Sept. 2006.

[2] P. Popovski and H. Yomo, "The Anti-Packets Can Increase the Achievable Throughput of a Wireless Multi-Hop Network," 2006 IEEE International Conference on Communications, pp. 3885-3890, 2006.

[3] L. You, S. C. Liew and L. Lu, "Reliable Physical-Layer Network Coding Supporting Real Applications," in IEEE Transactions on Mobile Computing, vol. 16, no. 8, pp. 2334-2350, 1 Aug. 2017.

[4] L. Lu, T. Wang, S. C. Liew and S. Zhang, "Implementation of physical-layer network coding," 2012 IEEE International Conference on Communications (ICC), 2012, pp. 4734-4740, 2012.

[5] L. Lu, S. C. Liew and S. Zhang, "Optimal Decoding Algorithm for Asynchronous Physical-Layer Network Coding," 2011 IEEE International Conference on Communications (ICC), pp. 1-6, 2011.

[6] L. Lu and S. C. Liew, "Asynchronous physical-layer network coding," IEEE Trans. Wireless Commun., vol. 11, no. 2, pp. 819–831, Feb. 2012.

[7] L. Lu, L. You, Q. Yang, T. Wang, M. Zhang, S. Zhang, and S. C. Liew, "Real-time implementation of physical-layer network coding," in Proc. the second workshop on Software Radio Implementation Forum (SRIF'13), pp. 71–76, 2013.

[8] S. Wang, Q. Song, Lei Guo and A. Jamalipour, "Constellation mapping for physical-layer network coding with M-QAM modulation," 2012 IEEE Global Communications Conference (GLOBECOM), pp. 4429-4434, 2012.

[9] V. Kumar, B. Cardiff and M. F. Flanagan, "Physical-layer network coding with multiple antennas: An enabling technology for smart cities," 2017 IEEE 28th International Symposium on Personal, Indoor, and Mobile Radio Communications (PIMRC), pp. 1-6, 2017.

[10] 3GPP TS 38.901. Study on Channel Model for Frequencies from 0.5 to 100 GHz (Release 17) V17.0.0; Technical Report; Rep. TR 38.901; 3GPP: Sophia Antipolis, France, 2022.

[11] M. Lu, Z. Shen, D. Guo and X. Wang, "A new physical layer network coding de-noising mapping based on M-QAM," 2017 First International Conference on Electronics Instrumentation & Information Systems (EIIS), pp. 1-5, 2017.

[12] V. T. Muralidharan and B. S. Rajan, "Distributed space time coding for wireless two-way relaying," IEEE Trans. Signal Process., vol. 61, no. 4, pp. 980–991, Feb. 2013.

[13] H. Yan, H. H. Nguyen and J. Su, "Distributed Precoding for OFDM in Two-Way Relaying Communications," in IEEE Transactions on Vehicular Technology, vol. 64, no. 5, pp. 1930-1941, May 2015.

[14] G. Bartoli, R. Fantacci, D. Marabissi and R. Simoni, "Physical Layer Network Coding in Multipath Channel: Effective Precoding-Based Transmission Scheme," 2011 IEEE Global Telecommunications Conference - GLOBECOM 2011, pp. 1-5, 2011.

[15] Y. Tan, S. C. Liew and T. Huang, "Mobile Lattice-Coded Physical-Layer Network Coding with Practical Channel Alignment," in IEEE Transactions on Mobile Computing, vol. 17, no. 8, pp. 1908-1923, 1 Aug. 2018.

[16] S. Denno, K. Yamamoto, & Y. Hou, "Precoded physical layer network coding with coded modulation in MIMO-OFDM bi-directional wireless relay systems," IEICE Transactions on Communications, Vol. E104-B, No. 1, pp. 99-108, 2021.

[17] T. Koike-Akino, P. Popovski, and V. Tarokh, "Optimized constellations for two-way wireless relaying with physical network coding," IEEE J. Select. Areas in Commun., vol. 27, pp. 773–787, June 2009.

[18] V. Namboodiri, V. T. Muralidharan, and B. S. Rajan, "Wireless bidirectional relaying and Latin squares," in Proc. IEEE Wireless Commun. and Networking. Conf., (Paris, France), pp. 1404–1409, Apr. 2012.

[19] D. Incebacak, H. Yanikomeroglu and B. Tavli, "Trade-offs in sum-rate maximization and fairness in relay-enhanced OFDMA-based cellular networks," 2014 IEEE Global Communications Conference, pp. 4770-4775, 2014.

[20] S. M. M. Yang, Modern Digital Radio Communication Signals and Systems. Cham, Switzerland: Springer, 2nd Edition, 2021.

[21] Z. Zhao, X. Cheng, M. Wen, B. Jiao and C. -X. Wang, "Channel Estimation Schemes for IEEE 802.11p Standard," in IEEE Intelligent Transportation Systems Magazine, vol. 5, no. 4, pp. 38-49, winter 2013.